International Journal of Nanomedicine

Dovepress
open access to scientific and medical research

Open Access Full Text Article

ORIGINAL RESEARCH

Nanosuspension-Loaded Dissolving Microneedle Patches for Enhanced Transdermal Delivery of a Highly Lipophilic Cannabidiol

Aguo Cheng[1,2], Suohui Zhang[1,3], Fanda Meng[4], Mengzhen Xing[5], Han Liu[3], Guozhong Yang[3], Yunhua Gao[1–3]

[1]Key Laboratory of Photochemical Conversion and Optoelectronic Materials, Technical Institute of Physics and Chemistry of Chinese Academy of Sciences, Beijing, People's Republic of China; [2]University of Chinese Academy of Sciences, Beijing, People's Republic of China; [3]Beijing CAS Microneedle Technology Ltd, Beijing, People's Republic of China; [4]School of Clinical and Basic Medical Sciences, Shandong First Medical University & Shandong Academy of Medical Sciences, Jinan, Shandong Province, People's Republic of China; [5]Key Laboratory of New Material Research Institute, Department of Pharmaceutical Research Institute, Shandong University of Traditional Chinese Medicine, Jinan, Shandong Province, People's Republic of China

Correspondence: Yunhua Gao, Key Laboratory of Photochemical Conversion and Optoelectronic Materials, Technical Institute of Physics and Chemistry of Chinese Academy of Sciences, Beijing, People's Republic of China, Tel +86 (10)82543581, Email yhgao@mail.ipc.ac.cn

Purpose: Transdermal Drug Delivery System (TDDS) offers a promising alternative for delivering poorly soluble drugs, challenged by the stratum corneum's barrier effect, which restricts the pool of drug candidates suitable for TDDS. This study aims to establish a delivery platform specifically for highly lipophilic drugs requiring high doses (log P > 5, dose > 10 mg/kg/d), to improve their intradermal delivery and enhance solubility.

Methods: Cannabidiol (CBD, log P = 5.91) served as the model drug. A CBD nanosuspension (CBD-NS) was prepared using a bottom-up method. The particle size, polydispersity index (PDI), zeta potential, and concentration of the CBD-NS were characterized. Subsequently, CBD-NS was incorporated into dissolving microneedles (DMNs) through a one-step manufacturing process. The intradermal dissolution abilities, physicochemical properties, mechanical strength, insertion depth, and release behavior of the DMNs were evaluated. Sprague-Dawley (SD) rats were utilized to assess the efficacy of the DMN patch in treating knee synovitis and to analyze its skin permeation kinetics and pharmacokinetic performance.

Results: The CBD-NS, stabilized with Tween 80, exhibited a particle size of 166.83 ± 3.33 nm, a PDI of 0.21 ± 0.07, and a concentration of 46.11 ± 0.52 mg/mL. The DMN loaded with CBD-NS demonstrated favorable intradermal dissolution and mechanical properties. It effectively increased the delivery of CBD into the skin, extended the action's duration in vivo, and enhanced bioavailability. CBD-NS DMN exhibited superior therapeutic efficacy and safety in a rat model of knee synovitis, significantly inhibiting TNF-α and IL-1β compared with the methotrexate subcutaneous injection method.

Conclusion: NS technology effectively enhances the solubility of the poorly soluble drug CBD, while DMN facilitates penetration, extends the duration of action in vivo, and improves bioavailability. Furthermore, CBD has shown promising therapeutic outcomes in treating knee synovitis. This innovative drug delivery system is expected to offer a more efficient solution for the administration of highly lipophilic drugs akin to CBD, thereby facilitating high-dose administration.

Keywords: nanosuspension, highly lipophilic drugs, dissolving microneedle, cannabidiol, knee synovitis

Introduction

The poor solubility of many current drugs and drug candidates presents a significant challenge within the pharmaceutical industry.[1] Approximately 40% of recently marketed drug compounds exhibit limited solubility in water, complicating their development and production processes.[2,3] The low solubility often leads to reduced dissolution rates, adversely affecting the bioavailability and absorption of orally administered drugs.[4,5]

Received: 1 December 2023
Accepted: 11 April 2024
Published: 7 May 2024

Graphical Abstract

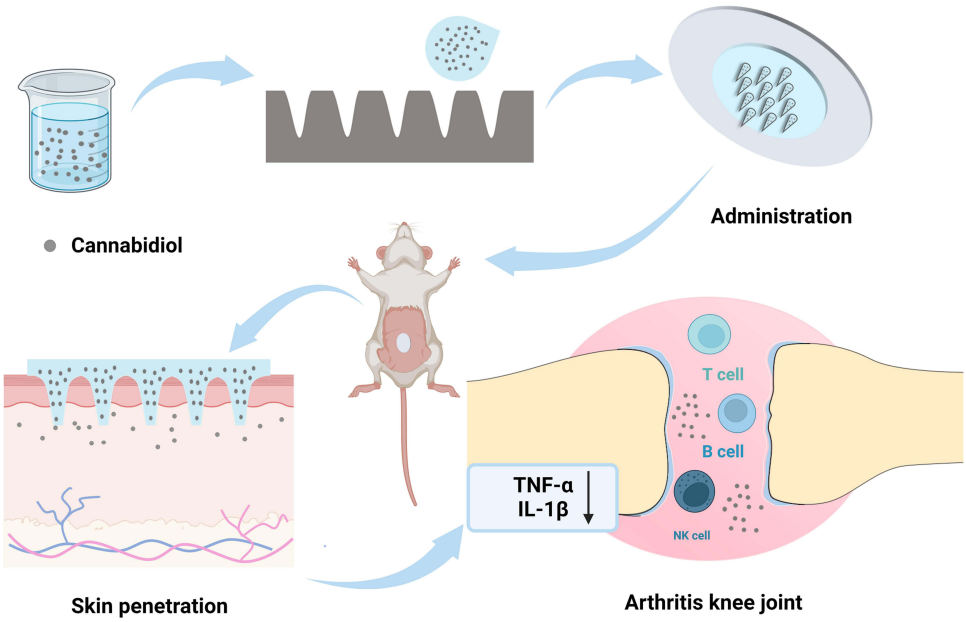

To exploit the therapeutic potential of poorly soluble drugs, several solubility enhancement strategies are employed, including nanoparticle systems, solubilization with cosolvents and surfactants, amorphous forms, solid dispersions, cocrystals, polymeric micelles, inclusion complexes, pH adjustments, salt forms, and liposomes.[6,7] Beyond mere solubilization, research is increasingly directed toward advanced delivery systems aimed at not only improving the bioavailability of poorly soluble agents but also enhancing patient compliance.[8] These systems address issues such as frequent dosing, swallowing difficulties, and needle phobia, offering controlled, targeted, or regulated delivery. Among these, the transdermal drug delivery system (TDDS) has garnered significant interest.[9]

TDDS enable drugs to bypass the liver's first-pass effect by penetrating the skin barrier into systemic circulation, often requiring lower therapeutic doses than traditional methods.[10] They allow for controlled drug release, maintaining stable plasma concentrations, which can mitigate side effects and variability among patients. This route simplifies administration without medical personnel and reduces the influence of gastrointestinal pH variations.[11,12] However, the barrier effect of the stratum corneum (SC) and the limited number of hair follicles and sebaceous glands restrict TDDS effectiveness, especially for drugs with high lipophilicity.[13] Traditionally, ideal candidates for TDDS are those with a molecular weight of less than 500 Da, a log P value between 1 and 3, and a daily dose of less than 10 mg/kg.[14,15] This narrows the scope of drugs suitable for TDDS, particularly for highly lipophilic drugs (log P > 5), whose transdermal delivery is hampered by low permeability.[16] To overcome these limitations, various passive and active technologies have been developed to enhance TDDS penetration and expand the range of suitable drug candidates.[10]

Microneedles (MNs) are emerging as scalable and commercially viable technology.[17] As third-generation TDDS, they typically ranging from 150 to 1500 μm in length and can penetrate the SC of the skin to create micron-sized pores for drug delivery.[18,19] For poorly soluble drugs, dissolving microneedles (DMNs) are particularly advantageous for long-term treatment due to their excellent biodegradability and compatibility.[20,21] However, the integration of poorly soluble drugs into the aqueous solution of DMN matrix materials often faces challenges, such as uneven drug dispersion within the DMN matrix.[22] Additionally, the loading dose of drugs in DMNs is often frequently constrained by their low solubility. The use of organic solvents to enhance drug solubility may also raise safety concerns regarding MNs.[23] Consequently, for highly lipophilic drugs that require high doses, developing a method for achieving homogeneous dispersion in MNs, thereby ensuring sustained delivery and improved bioavailability, is crucial.

Nanosuspensions (NS), or nanocrystals (NC), are proposed as a promising solution to this challenge. They facilitate a more uniform particle size distribution for lipophilic drugs when combined with DMN.[24,25]. Compared to other systems like nanoliposomes, nano micelles, and self-emulsifying systems, NS offers a high drug-loading capacity with minimal use of surfactants.[26–28] NS can create a concentration gradient with the epidermal layer, enhancing passive diffusion; it also has potential for hair follicle targeting, making it conducive to forming a reservoir for continuous drug delivery.[29]

Cannabidiol (CBD, log P = 5.91) served as a model drug to demonstrate the combined use of DMN and NS technology for high-dose, sustained intradermal delivery of highly lipophilic drugs (Figure 1). CBD is a non-psychoactive and essentially non-toxic compound derived from the cannabis plant.[30] It has been approved by the FDA for treating refractory epilepsy and exhibits promising therapeutic effects in analgesia, inflammation, and neurodegenerative disorders.[31–33] The interaction of CBD with CB2 receptors, primarily found in immune cells, leads to reduced inflammatory responses, positioning it as a potential treatment for synovitis-associated pain and inflammation.[34] Additionally, CBD has been shown to suppress the release of pro-inflammatory cytokines, such as TNF-α and IL-6. In various conditions like collagen-induced arthritis, osteoarthritis, monoarthritis, and carrageenan-induced joint swelling, CBD has shown effective therapeutic outcomes with minimal side effects.[35–38] Despite its general tolerance and minimal side effects, CBD's hydrophobic nature and unstable absorption in the gastrointestinal system can lead to unpredictable pharmacokinetics.[10,39,40] Oral administration of CBD is particularly affected by significant first-pass metabolism in the liver, resulting in approximately only 6% bioavailability.[41] These limitations substantially restrict CBD's therapeutic application in clinical settings.

In this study, the bottom-up method was used to reduce the particle size of CBD, enhancing solubility through CBD-NS, which was then incorporated into DMN. The dissolution, physicochemical, and mechanical properties of DMN were characterized, and the release behavior in vitro of CBD-NS DMN was evaluated. Sprague-Dawley (SD) rats were used to assess the efficacy of the DMN patch in treating knee synovitis, along with its skin permeation kinetics and pharmacokinetic profiles. The aim of this work was to provide a platform for highly lipophilic drugs that require high-dose administration and contribute to improving their skin permeability and bioavailability.

Materials and Methods

Materials and Animals

Cannabidiol (CBD) with a purity of ≥99.0% was sourced from Yunnan Hansu Biotechnology Co., Ltd., (Kunming, China). Polysorbate 80 (Tween 80), Pluronic® F-127 (P127), and ammonium acetate (with a purity of ≥99.0%, LC-MS grade) were acquired from Sigma-Aldrich (Shanghai, China). Hydroxypropyl methylcellulose (HPMC) was purchased from Anhui Sunhere Pharmaceutical Excipients Co., Ltd. (Huainan, China). Polyvinylpyrrolidone (PVP K30) was procured from Gobekie (Shanghai, China) and trehalose was acquired from HAYASHIBARA Co., Ltd (Okayama, Japan). Hyaluronic acid (HA, 50–100 kDa) was furnished by Freda Biotechnology Co., Ltd (Jinan, China). The HPLC-grade solvents, methanol, and acetonitrile (ACN), were obtained from Thermo Fisher Scientific Inc (Waltham, MA, USA). All other chemicals utilized in the experiment were of analytical grade.

The study was conducted using male SD rats, sourced from SPF Biotechnology Co., Ltd. (Beijing, China), with an average body weight of 250 ± 20 g.

All animal studies were approved by the Institutional Animal Care and Utilization Committee of the Institute of Physics and Chemistry, Chinese Academy of Sciences (CAS). The methods were carried out in accordance with the guidelines in the Guide for the Care and Use of Laboratory Animals (Eighth Edition, 2011).

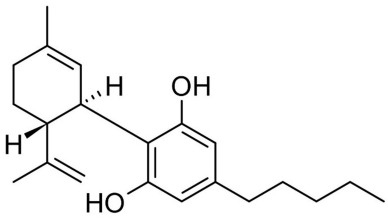

Figure 1 Chemical structures of CBD.

Preparation and Characterization of CBD-NS

CBD-NS were produced by antisolvent precipitation in a bottom-up method, as described in previous studies.[42,43] A stock solution was prepared by dissolving 300 mg of CBD in 1 mL of ethanol as shown in Figure 2 and then slowly added into 5 mL of aqueous Tween 80, P127, or HPMC solution (3% w/w). In this process, an ultrasonic dispersion instrument (JY 92-IIN, Xinzhi Biotechnology Co., Ltd., Ningbo, China) was used for continuous ultrasonic treatment, and the ice bath was applied to maintain the temperature to prevent overheating. The instrument used a No.6 probe for ultrasonic treatment at an amplitude of 30% for 10 min (time interval of 10s). The organic solvent was removed by magnetic stirring to obtain the final CBD-NS (CBD theoretical concentration is 60 mg/mL).

The particle size, polydispersity index (PDI), and zeta potential of NS were measured by dynamic light scattering (DLS, Nano ZS 90, Malvern, Panalytical, UK).[44] The CBD-NS sample was diluted 50 times with deionized (DI) water before observation. The analysis was performed at room temperature (25 ± 2°C) in triplicate. Similarly, the diluted samples were examined using scanning electron microscopy (SEM) and transmission electron microscopy (TEM).[44,45] 7 μL of the diluted CBD-NS sample was dropped onto a smooth silicon wafer and allowed to dry naturally. It was then coated with gold using sputtering gold plating equipment, and the particle morphology was observed by SEM (S-4800, Hitachi, Tokyo, Japan) at an accelerating voltage of 10 kV. Additionally, 7 μL of the diluted CBD-NS sample was placed onto a copper grid covered with a plain carbon support film and left to dry overnight at room temperature. These samples were then viewed by TEM (HT7700, Hitachi, Tokyo, Japan) at an accelerating voltage of 100 kV.

The CBD-NS was collected, diluted 100-fold with ACN, filtered through a 0.22 μm filter, and its concentration was determined by HPLC.

Fabrication and Characterization of CBD-NS DMN

Fabrication of CBD-NS DMN

The DMN was fabricated using a one-step manufacturing process. Specifically, 1 g of CBD-NS was added to a centrifuge tube, followed by the addition of 11.60% (w/w) HA (50–100 kDa), 5% (w/w) PVP K30, and 0.4% (w/w) trehalose. These components were mixed thoroughly and then centrifuged at 5000 rpm for 5 min to ensure the removal of air bubbles (Figure 2). Despite the centrifugal method used to remove the bubbles, the matrix solution has sufficient viscosity to stabilize CBD-NS without causing it to settle.

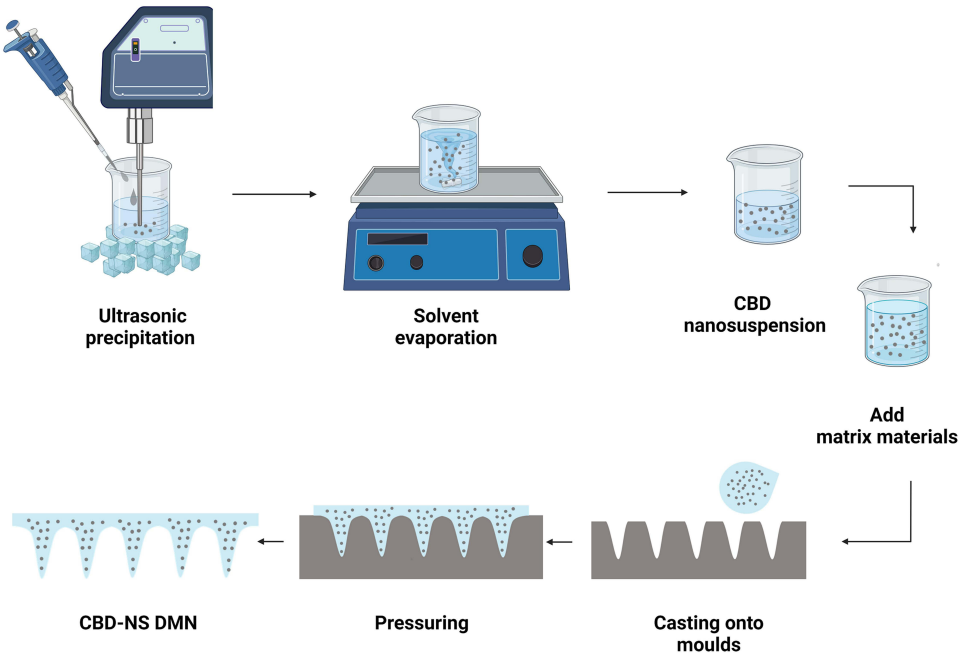

Figure 2 The scheme of CBD-NS and CBD-NS DMN preparation.

SEM Analysis

Prior to SEM observation, a row of needles was cut off using a lancet, and the needles were fixed to an L-shaped table using conductive adhesive. The tip appearance of the needles was observed by SEM after the needles were sprayed with gold. The SEM accelerating voltage was 10 kV.

Dissolution Abilities

The dissolution capabilities of DMNs at varying times were evaluated using isolated pig skin (Schematic operation Figure S3). The skin was removed from a −20°C refrigerator, subsequently thawed, and stabilized in a 37°C PBS solution (pH=7.4) for 30 min. The surface of the skin was then gently blotted with filter paper to remove excess moisture. Finally, the DMNs were administered to the prepared porcine skin surface utilizing a special needle feeder, ensuring uniform application and optimal skin penetration. After 1 min, 5 min and 10 min, the DMNs were removed, and the tip changes were observed under a microscope (SMZ18, Nikon, Tokyo, Japan).

Mechanical Properties

The mechanical properties of the CBD-NS DMN were evaluated through a displacement-force test (1220SB, SA Precision Instruments Co., Ltd., Shanghai, China).[46] In brief, to assess the DMN patch's resistance to compression, a single patch was secured on a rigid stainless-steel platform, oriented with the DMN side facing upwards. It was then compressed by a sensor probe measuring 2×2 mm, moving vertically at a speed of 0.1 mm/s. The displacement-force test station recorded the curves continuously until reaching the maximum force threshold of 5 N.

Thermal Analysis

The thermal characteristics of the CBD-NS in combination with DMN were investigated through differential scanning calorimetry (DSC 3500 Sirius, NETZSCH, Bavaria, Germany).[47] The procedure involved incrementally heating the sample from 40°C to 250°C at a rate of 10°C/min. During this process, a purge gas (N_2) was flowed at 40 mL/min and a protective gas (N_2) was flowed at 60 mL/min to safeguard the sample.

Powder X-Ray Diffraction

To confirm the crystalline structure of CBD in the DMN, powder X-ray diffraction (XRD) analysis was performed.[47] The samples examined included CBD powder, Blank DMN (a composition of matrix materials without CBD), and CBD-NS DMN. These were analyzed separately in a rotating sample holder, with CBD in powder form and both Blank DMN and CBD-NS DMN in film form. The analyses utilized an X-ray diffractometer (D8 Focus, Bruker, Germany), scanning samples at a rate of 0.1° per step in continuous mode across a 2θ range of 5–60°.

Insert Depth of C6 DMN

Coumarin 6 (C6), a fluorescent probe with a similar molecular weight and log P (4.91) to CBD, was selected as the model drug. C6 DMN was prepared following the same procedure as CBD-NS DMN.[48] The DMN was pressed onto the porcine skin using a special needle feeder with a force of about 20 N for 10s. After removing the patch, the skin sample was placed on a glass slide and observed with a confocal laser scanning microscope (CLSM, ARsiMP-LSM, Nikon, Tokyo, Japan).[49] Z-axis scanning was performed from the SC of the skin sample to the dermis, layer by layer. The SC (z = 0 μm) was defined as the imaging plane, and the scanning speed was set at 20 μm/step.

Distribution of C6 in the Abdominal Skin

The distribution of C6 in the abdominal skin of SD rats was observed using an in vivo imaging system (photon imager optima, Biospace lab, Paris, France).[49] The prepared C6 DMN patch was inserted into the abdominal skin of anesthetized rats with appropriate force. The DMN patches were removed after 0, 1, 2, 4, 8, 12, and 24 h, and the fluorescence in the animals was directly observed by the imaging system. After 24 h of adhesion, the patches were removed, and then the rats were observed continuously up to 48 h.

In vitro Release

A modified Franz diffusion cell (912-SCT-S, Logan Instruments Corporation, Somerset, NJ, USA) was employed to understand the release performance of the CBD-NS DMN. The CBD-NS DMN (2.44 ± 0.07 mg CBD per patch) was wrapped in a dialysis bag with a molecular weight cutoff of 3500 Da (MD3533, Yuanye Bio-Technology Co., Ltd, Shanghai, China), with the needle tip facing downwards. The dialysis bag, containing 200 μL of receiving solution, was placed in a diffusion cell filled with 2.7 mL of 2% Tween 80-PBS. The system was magnetically stirred at 600 rpm at 32 ± 0.2°C. After 0, 1, 2, 4, 6, 8, 12, and 24 h, the solution was completely removed and replaced with an equal volume of fresh receiving solution. The samples were then filtered through a 0.22 μm filter, and the supernatant was analyzed by HPLC. The area of the CBD peak in the chromatogram was substituted into the equation of the standard curve of the day to determine the concentration of CBD in the sample solution.

Skin Permeation

In vivo Skin Permeation

To investigate the in vivo permeation of DMN patches, SD rats were anesthetized with isoflurane. Abdominal hair was shaved and then treated with depilatory cream. The abdominal hair was shaved and then treated with depilatory cream. DMN patches (2.44 ± 0.07 mg CBD per patch) were applied to the abdominal skin under appropriate pressure and secured with medical tape. The patches were removed at intervals of 2, 4, 8, 12, 16, and 24 h, respectively. A cotton swab was used to collect epidermal residue and was stored in the same Eppendorf (EP) tube as the removed DMN patches. Each sample had 3 mL of mobile phase added and was vortexed for 2 h. The samples were then filtered through a 0.22 μm filter for HPLC analysis.

To quantify the amount of CBD retained in the rat skin, skin samples were collected at four time points (8, 24, 48 and 72 h) post-application and analyzed for CBD content. The procedure was as follows: After 8 h of DMN patch application, the rats were euthanized, the patch removed, and the residue cleaned from the epidermis. A skin sample of approximately 0.5 cm^2 was excised from the application site. Following 24 h of application, the rats were divided into three groups: one group was sacrificed to remove skin tissue, euthanized to remove skin tissue; the second group was monitored until 48 h post-patch removal, at which point they were euthanized and the skin collected; the third group was euthanized at 72 h. Skin samples were stored at −80°C prior to processing.

Skin Samples Processing

Specific intradermal extraction involved making an incision in the skin with scissors, then weighing and recording the sample. Each sample was added to 3 mL of methanol and agitated for 24 h on a shaker, followed by sonication for 30 min, repeated twice. The supernatant was then filtered through a 0.22 μm filter into a vial for HPLC analysis.

Arthritis Modeling and Treatment

Modeling of Kaolin/λ-Carrageenan Induced Knee Synovitis

In accordance with established literature methods, rats were anesthetized with isoflurane prior to the induction of knee synovitis. Subsequently, hair around the knee joints was removed using depilatory cream, and the rats were then randomly divided into three distinct groups.[48,50] A suspension containing 4% kaolin and 2% λ-carrageenan was prepared. Following this, 100 μL of the suspension was injected into the synovial cavity of the rat knee joints. To ensure successful modeling, the right limb was subjected to repeated extension and flexion movements. Treatment began 24 h after the induction of knee synovitis, with administrations occurring once daily across 15 rats (n=5 per group): the negative control group received an injection of 0.1 mL saline (Model group); the positive control group was treated subcutaneously with methotrexate (MTX S.C., 1 mg/kg); and the CBD-NS DMN group received 10 mg/kg. The CBD-NS DMN patch was applied to the abdominal skin of the rats, pressed for 30s, and then secured with medical tape for 24 h before removal.

Measurements of the diameters of both the left and right knee joints in rats were taken on days 1, 3, 5, and 7 post-modeling using a vernier caliper. The formula used to calculate the degree of swelling in the right knee joint is as follows:

$$\text{Degree of Swelling} = \frac{(\text{Right Knee Joint Swelling} - \text{Left Knee Joint Swelling})}{\text{Left Knee Joint Swelling Degree}} \times 100\%$$

Inflammatory Factor Testing

On the final day of the experiment, serum samples were collected from each animal and stored at −80°C until analysis. ELISA kits for the detection of the inflammatory factors IL-β and TNF-α were provided by Solarbio (Beijing, China), and the experimental procedures were conducted following the manufacturer's instructions.

Histopathological Analysis

To assess the histological alterations in the knee synovitis, the rats were euthanized at the conclusion of the experiment to extract the right knee joints. These joints were first fixed in 10% (w/v) paraformaldehyde, followed by embedding in paraffin to prepare them for sectioning. To evaluate the histologic changes in the synovium and the extent of articular cartilage deterioration, the sections were stained using hematoxylin and eosin (H&E). This staining procedure highlights the cellular components and extracellular matrix, allowing for a detailed examination of inflammatory infiltration, synovial membrane thickening, and cartilage wear indicative of synovitis.

Pharmacokinetic Studies of CBD

Experimental Grouping and Administration

To evaluate the pharmacokinetics of CBD after oral administration and CBD-NS DMN, rats were randomly divided into two groups. Group 1 (oral CBD solution, n = 6) received a solution prepared by blending equal volumes of ethanol and Tween 80 with CBD. Water was then added to achieve a final ratio of $V_{ethanol}$: $V_{Tween\ 80}$: V_{DI} = 1:1:18) resulting in a CBD concentration of 10 mg/mL. Each rat in this group was administered a dose of 10 mg/kg via gavage. Group 2 (CBD-NS DMN administration group, n = 6) involved the depilation of rats using hair removal cream at the start of the experiment. Each rat then received one patch of CBD-NS DMN (2.44 ± 0.07 mg CBD per patch), equivalent to a dose of 10 mg/kg, applied to the abdomen and removed after 24 h.

Blood samples were collected from the tail vein at predetermined intervals (1, 2, 4, 8, 12, 24, 48, 60, and 72 h post-administration), with 100 μL of plasma obtained from each rat. These plasma samples were then stored at −80°C pending further analysis.

Plasma Sample Processing

Begin by adding 100 μL of rat plasma and 10 μL of the internal standard solution, which contains (-)-delta-9-THC-D3 at a concentration of 1 μg/mL, to an EP tube. Vortex the mixture for 1 min before adding 200 μL of an extractant—a 1:1 mixture of methanol and ACN. Vortex again for 1 min, followed by centrifugation at 10,000 rpm for 10 min. Analyze 100 μL of the resultant supernatant using UPLC-MS/MS.

Quantification of CBD

HPLC-UV Method

CBD quantification in vitro was carried out using an HPLC system (LC-20AT, Shimadzu, Kyoto, Japan) equipped with a YMC® C18 column (250 mm × 4.6 mm, 5 μm). The column temperature was maintained at 30°C, and detection was performed at a wavelength of 220 nm. The mobile phase consisted of ACN/ water in a 70/30 ratio, with a flow rate set at 1 mL/min.

UPLC-MS Method

For in vivo CBD analysis, UPLC-MS/MS was utilized, comprising an UltiMate 3000 autosampler (Dionex, Sunnyvale, CA, USA) coupled with a Q Exactive orbitrap mass spectrometer (Thermo Fisher Scientific, Waltham, MA, USA). Detection occurred via electrospray ionization (ESI) in negative ion mode, with quantitative analysis conducted in Target-SIM mode. Chromatographic separation was achieved on a Hypersil GOLD™ column (100 mm × 2.1 mm, 3 μm) with the column temperature set at 35°C. The mobile phase was composed of 2 mM ammonium acetate in water (phase A) and ACN (phase B), with an A:B ratio of 20:80 and a flow rate of 0.2 mL/min.

Statistical Analysis

Data analysis was conducted using GraphPad Prism software version 9.4.1 (GraphPad Software, LLC., San Diego, USA). All data were presented as mean ± standard deviation (S.D.). Pharmacokinetic parameters were evaluated using DAS 2.0 software (Chinese Society of Pharmacology and Pharmacy, China).

Results

Characterization of CBD-NS

CBD-NS were successfully synthesized using the anti-solvent precipitation technique. To optimize the formulation, three commonly utilized stabilizers were evaluated: Tween 80, P127 and HPMC E5. Tween 80, a non-ionic surfactant, can interact with poorly soluble drugs through hydrogen bonding or van der Waals forces, thus preventing nanoparticle aggregation. P127, an amphiphilic copolymer consisting of hydrophilic polyethylene oxide (PEO) and hydrophobic polypropylene oxide (PPO) blocks, encapsulates drug crystals with its PEO segments to offer steric hindrance against particle aggregation, with the hydrophobic PPO chains driving adsorption to the crystal surface. HPMC, a widely used cellulose derivative in pharmaceutical nanocrystals, enhances oral drug delivery as a hydrophilic polymer.[51]

As demonstrated in Figure 3A and B, when Tween 80 was used as a stabilizer, the average particle size of CBD measured by DLS was 166.83 ± 3.33 nm, and PDI was 0.21 ± 0.07. Conversely, when P127 or HPMC served as the stabilizer, the average particle size exceeded 300 nm and the PDI surpassed 0.3, indicating suboptimal dispersion of CBD. Additionally, the Zeta potential of the Tween 80-stabilized system was −38.13 ± 0.25 mV, compared to −26.93 ± 0.60 mV and −17.2 ± 0.23 mV for the P127 and HPMC systems, respectively. Typically, a zeta potential of at least −30 mV is indicative of physical stability in NS, underscoring Tween 80's superiority in stabilizing CBD.[52] Consequently, Tween 80 was selected for subsequent CBD-NS preparations due to its enhanced stability and efficiency in reducing drug particles to the nanoscale. Figures 3E and F depict the CBD-NS as regular nanoparticles with diameters ranging from 100 to 500 nm, aligning with DLS measurements.

The concentration of CBD-NS, determined by HPLC, was 46.11 ± 0.52 mg/mL. Compared to the theoretical concentration of 60 mg/mL, the encapsulation efficiency of CBD achieved with this method was calculated to be

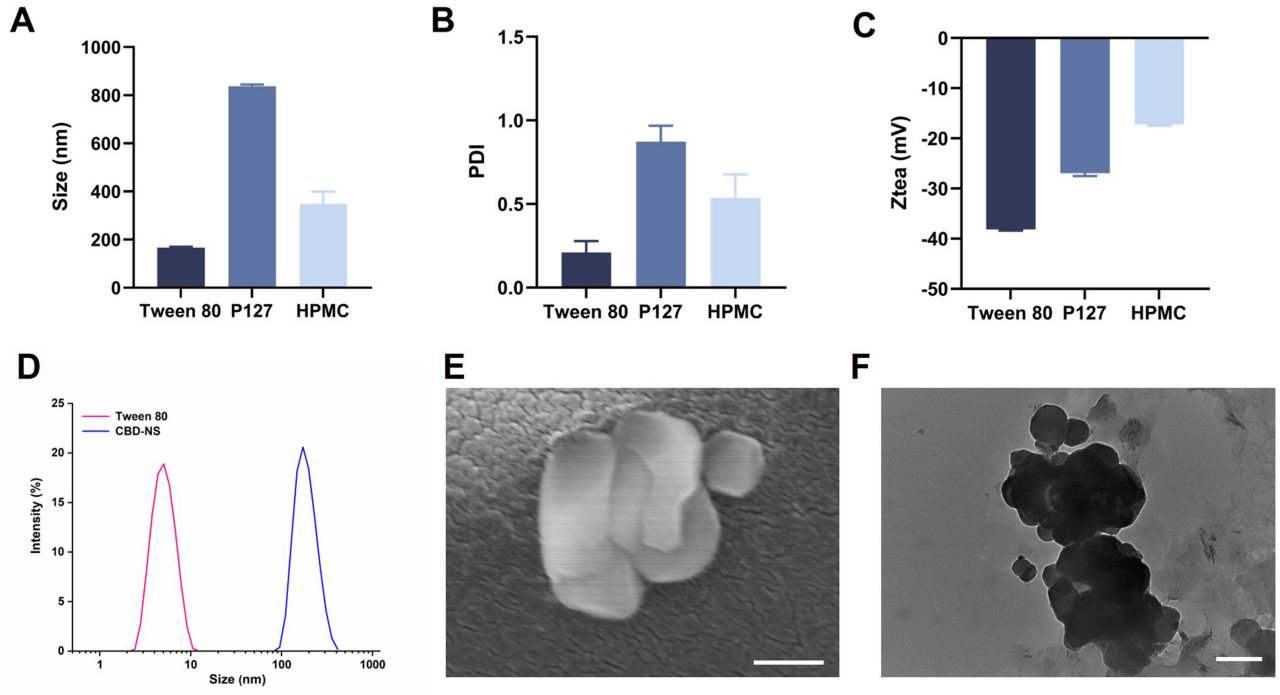

Figure 3 Different formulations of (**A**) the particle size; (**B**) PDI (**C**) zeta potential; (**D**) the particle size distributions; (**E**) magnification 100 kx SEM image and (**F**) magnification 100 kx TEM image of Tween 80-CBD-NS, scale bar = 200 nm.

75.85 ± 0.87%. Notably, the solubility of CBD in water is significantly low, falling below the detection limit of our HPLC method (0.1 μg/mL); literature sources report its aqueous solubility to be 0.063 μg/mL.

Characterization of CBD-NS DMN

Through a meticulous screening process (illustrated in Figures S1 and S2), we identified an optimal formulation comprising 11.6% (w/w) HA 50–100 kDa, 5% (w/w) PVP K30 and 0.4% (w/w) trehalose for the preparation of CBD-NS DMN. The patches were designed with a circular shape, 1 cm in diameter, featuring an array of 145 needles. SEM images (Figure 4A and B) reveal that each needle, measuring 500 μm in both height and spacing, is conically shaped. Remarkably, the SEM images at 5000× magnification displayed no particulate matter for the Blank DMN, while the CBD-NS DMN showcased nanoparticles ranging from 300–500 nm, uniformly dispersed throughout. This uniform dispersion indicates an effective integration of CBD-NS into the DMN, albeit with a slight increase in particle size, possibly due to the adsorption of the matrix material.

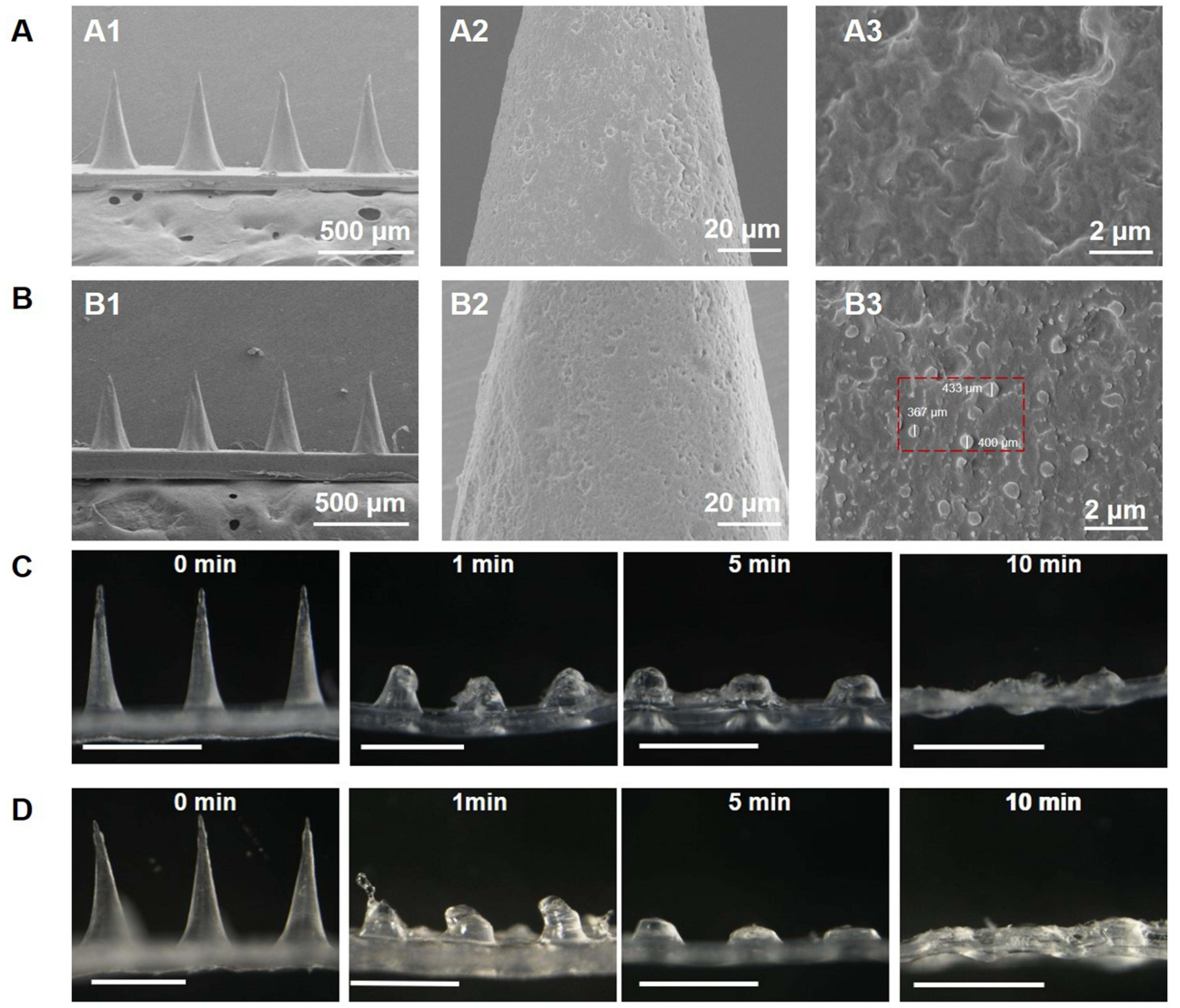

Figure 4 (**A**) SEM images of Blank DMN (A1) magnification 60x; (A2) magnification 1000x and (A3) magnification 5000x. (**B**) CBD (pure drug). (**B**) Scanning microscopy images of CBD-NS DMN (B1) magnification 60x; (B2) magnification 1000x and (B3) magnification 5000x. (**C**) Images of Blank DMN dissolution in skin over time (C1) 0 min; (C2) 1 min; (C3) 5 min and (C4) 10 min, scale bar = 500 μm. (**D**) Images of CBD-NS DMN dissolution in skin over time (D1) 0 min; (D2) 1 min; (D3) 5 min and (D4) 10 min, scale bar = 500 μm.

The dissolution ability of Blank DMN and CBD-NS DMN in isolated porcine skin were also examined. From Figure 4C and D, it can be seen that the tips of the DMN gradually dissolved as the insertion time increased. After 1 min of inserted, the tips were almost 50% dissolved in the skin, and within 10 min, the tips were almost completely dissolved. Notably, the dissolution rates between Blank DMN and CBD-NS DMN were comparable, suggesting that the incorporation of CBD-NS did not detrimentally affect the material's dissolution properties.

To determine if the DMN patches possess the necessary mechanical strength to penetrate the skin under pressure, we analyzed the displacement-force curve of the CBD-NS DMN, as depicted in Figure 5A. The absence of any significant deflection points in this curve indicates that none of the needle tips broke within the tested range.[53] Literature indicates that a microneedle is considered capable of penetrating the skin without breaking if it can withstand an axial force greater than 0.15 N.[54] Based on these criteria, our DMN patches demonstrated robust mechanical properties, proving adequate for effective skin penetration.

As shown in Figure 5B, the DSC curve of CBD exhibited a sharp endothermic peak at 69.3°C, which was consistent with the documented melting point of CBD.[55] While the CBD-NS DMN did not exhibit any melt heat absorption at 69.3°C. Similar to the Blank DMN without CBD-NS loading, they had a broad heat absorption peak in the temperature range of 100–140°C, indicating that the prepared CBD-NS was amorphously dispersed in the MN matrix material.

XRD was used to compare the crystalline form of CBD-NS in DMN, and the comparative diffractograms of pure CBD drug, blank DMN without CBD-NS, and CBD-NS DMN are shown in Figure 5C. The pure CBD exhibited clear crystalline diffraction peaks, consistent with prior findings, demonstrating its crystalline nature.[28] Although there were no crystalline peaks observed for the Blank DMN, this was attributable to the fact that the matrix of blank DMN consisted of HA, PVP, and trehalose, which remained in an amorphous state after the manufacture of DMN. In contrast, characteristic diffraction peaks of CBD (9.7°, 13.4° and 17.4°) appeared in CBD-NS DMN, suggesting that CBD-NS maintained a certain degree of crystallinity after loading into the DMN. This is different from the result of DSC, which may be due to the low concentration of CBD-NS after loading into DMN, resulting in that DSC could not detect the melting peaks of CBD-NS.

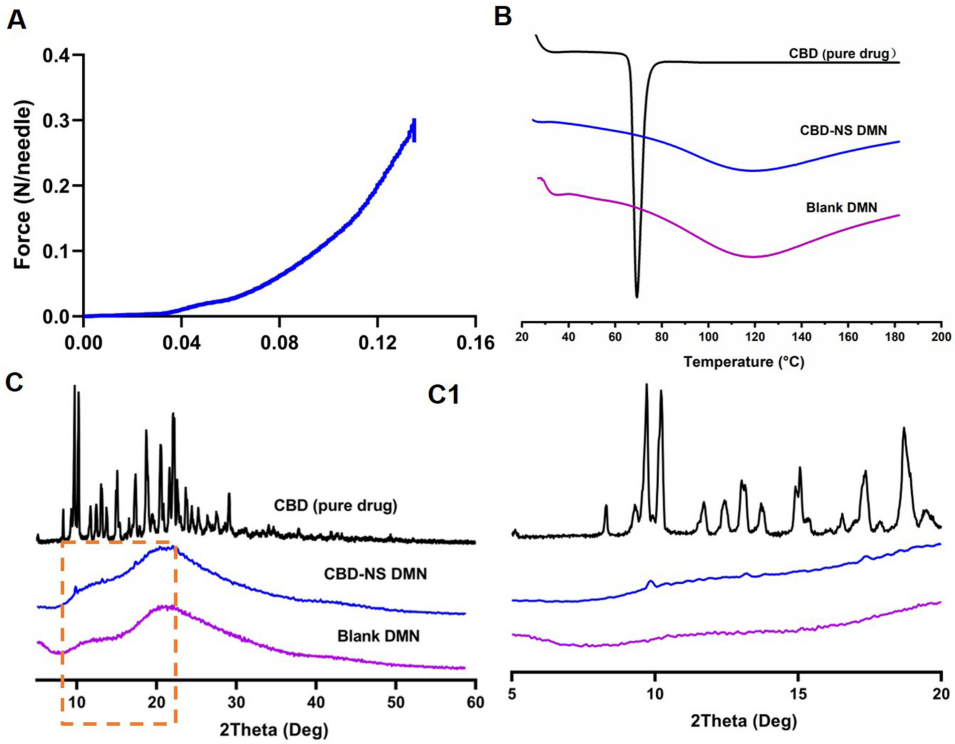

Figure 5 (**A**) Mechanical performance of CBD-NS DMN. (**B**) DSC analysis of CBD (pure drug), Blank DMN and CBD-NS DMN. (**C**) XRD analysis of CBD (pure drug), Blank DMN and CBD-NS DMN. (C1) 2 Theta range 5–60° and (C2) 2 Theta range 5–20°.

Insert Depth and Distribution of C6 in the Skin

To evaluate the ability and depth of DMN insert into the skin in vitro, C6 DMN was embedded into isolated porcine skin. After 20s action time, the DMN was removed, and its images were examined under bright field and fluorescence, respectively. The skin was then scanned by CLSM, and finally, the insert depth of the C6 DMN was reconstructed in 3D. As shown in Figure 6A, clear arrays remained on the pig skin by DMN, indicating good penetration ability. The DMN delivered C6 to a depth of 200–300 μm (Figure 6B).

Given that CBD lacks functional groups amenable to fluorescent labeling, C6 was employed as a surrogate to study the diffusion behavior of highly lipophilic drugs within the abdominal skin using the DMN system. In vivo imaging system showed that with prolongation of DMN action time, the fluorescence intensity of the drug on the skin surface gradually decreased and spread to the skin. After the patch was removed at 24 h, there was almost no drug content observed at 48 h (Figure 6C). These findings demonstrate that C6 DMN not only achieve sustained skin residency but also highlight the system's applicability for future delivery of more lipophilic drugs.

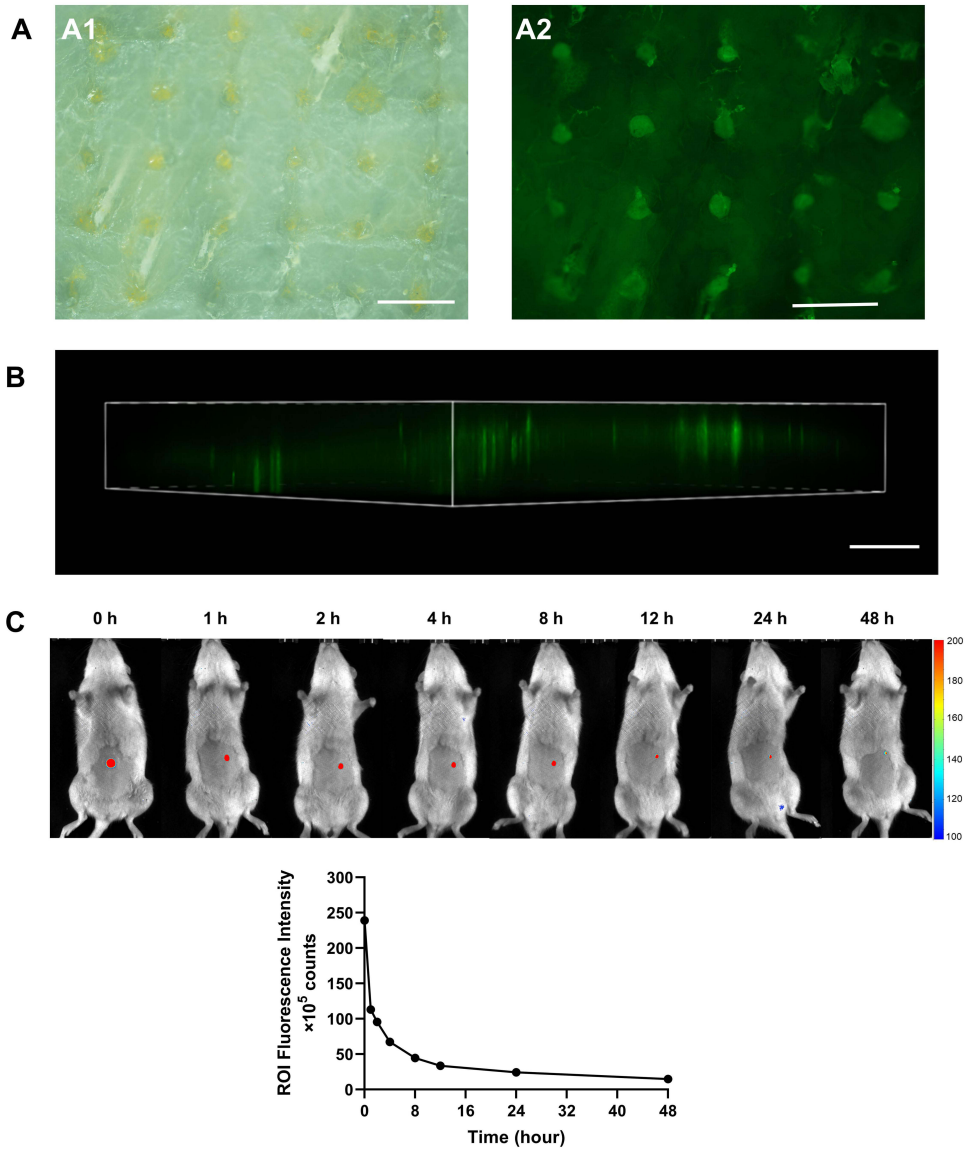

Figure 6 (**A**) Images of porcine skin after treatment with C6 DMN (A1) Bright-field image; (A2) Fluorescence microscopy. (**B**) Insert depth obtained by CLSM 3D reconstruction, scale bar = 500 μm. (**C**) In vivo imaging of rats after being treated with C6, (C1) In vivo images throughout 48 h and (C2) the curve of fluorescence intensity with time.

https://doi.org/10.2147/IJN.S452207 DovePress

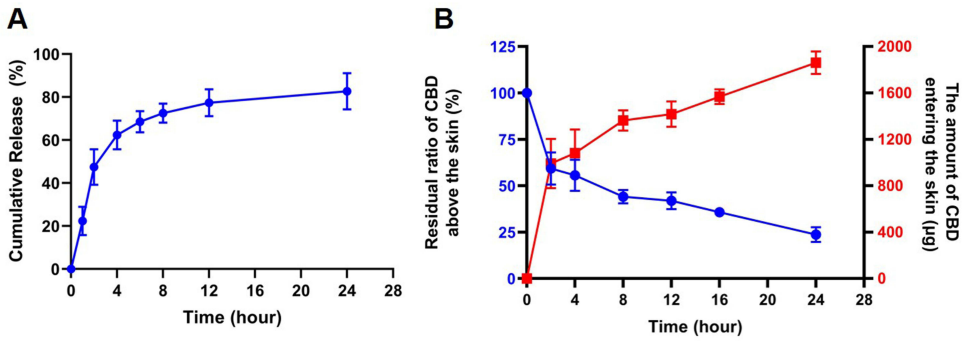

Figure 7 (**A**) In vitro cumulative release curve of CBD-NS DMN in 2% Tween 80. (**B**) The residual ratio of CBD above the skin (blue line), and the accumulative amount of CBD entering the skin (red line). Data are represented as mean ± S.D., n = 4.

Vitro Release

In vitro drug release was performed to evaluate the CBD-NS DMN. As CBD is a lipophilic drug, the selected receiving medium should ensure the sink condition. After screening, 2% Tween 80-PBS solution was chosen because it had a CBD solubility of 10.13 ± 1.06 mg/mL and the maximum solubility of each patch (2.44 mg CBD per patch) in the receiving solution was 0.90 mg/mL, so 2% Tween 80-PBS was able to satisfy the sink condition. From the in vitro release curve (Figure 7A), it can be seen that the CBD-NS DMN was released rapidly within the first 2 h with a cumulative release ratio of 47.45 ± 8.25% to 72.50 ± 4.43% at 8 h, then the release tended to level off, with a cumulative release ratio up to 82.67 ± 8.45% after 24 h. Several models were fitted to the in vitro release curve of CBD-NS DMN as shown in Table 1. The CBD-NS DMN release kinetics were best represented by the first-order model, with an R^2 of 0.9844.

Skin Permeation

This study aimed to evaluate the ability of CBD-NS DMN to deliver the drug into the skin and retain it at the site.[56] The transdermal absorption was quantified by measuring the residual CBD in rat skin. Initial findings Figure 7B showed that transdermal delivery was predominantly facilitated by DMN dissolution, with a residual CBD rate of 59.35 ± 8.70% at 2 h and 44.14 ± 3.55% at 8 h corresponding to a skin penetration amount of 61.36 ± 67.44 μg. Since then, the release rate has slowed down to 23.71 ± 3.98% CBD residue at 24 h, and the amount entering the skin exceeded 1600 μg.

The amount of CBD deposited at the site of skin action was also detected at 8, 24, 48 and 72 h. It can be seen from Table 2, that after DMN delivery of CBD-NS to the skin, the drug could be retained in the application site of the skin. However, no CBD content was detected in the skin at 72 h, indicating that after the patch was removed at 24 h the CBD residing in the skin was gradually delivered into systemic circulation. By measuring the patch residue rate, the method for calculating CBD skin entry is consistent with the data released in vitro. Specifically, the delivery rate of CBD-NS DMN can reach 80% within 24 h.

Table 1 Fitting of in vitro Release Test Curves

Fitting Model	CBD-NS DMN	
	Equation	R^2
Zero-Order	Q_t=1.72t+40.03	0.5036
First-Order	Q_t=81.28 (1-$e^{-0.3588t}$)	0.9844
Higuchi	Q_t=13.62$t^{1/2}$+21.39	0.7718
Ritger-Peppas	Q_t= 40.21$t^{0.23}$	0.9219

Table 2 CBD Concentration in the Skin After CBD-NS DMN Administration at the Application Site (Mean ± S.D., n = 4)

Time (h)	CBD Concentration in the Skin (μg/g)
8	532.02 ± 173.84
24	601.43 ± 360.01
48	150.15 ± 66.11
72	NA

Pharmacodynamic Study of CBD-NS DMN in Arthritis Model

Treatment of Rat Model of Knee Synovitis Induced by Kaolin/λ-Carrageenan

To assess the severity of knee synovitis, the swelling of the right knee joint of rats was adopted as a direct indicator. The positive control group received MTX for drug treatment to compare the therapeutic effects of CBD with clinically for knee synovitis.[48] As shown in Figure 8A and B, following a single day of injecting kaolin/λ-carrageenan into the right synovial cavity, significant swelling of the knee joint was noted. This swelling was approximately 25–30% larger than the normal left knee, suggesting the successful establishment of the knee synovitis model. The administrations were then performed, with each group receiving one dose per specified time frame. By the third day, the swelling in both MTX S.C. and CBD-NS DMN groups had decreased, while no observable change was noted in the Model group. On the fifth day, the swelling in both MTX S.C. and CBD-NS DMN groups was significantly reduced, with the CBD-NS DMN showing superior therapeutic effects compared to the MTX S.C. group. It is important to note that the swelling level in the Model group increased, likely due to disease recurrence without drug treatment. By the seventh day, the CBD-NS DMN group's swelling level had decreased to 4.41%.

Weight Monitoring

From the body weight test (Figure 8C), it was found that the rest of the rats except for the MTX S.C group gained some weight after one week, while the body weight of rats in the MTX group decreased and there were deaths of rats at the end of treatment. Although similar therapeutic effects can be achieved with MTX, there is some toxicity of MTX. In terms of safety considerations, CBD-NS DMN is superior to MTX.

CBD-NS DMN Inhibits Inflammatory Cytokines

In this experiment, ELISA kits were used to detect the concentration of TNF-α and IL-1β in rat serum to verify the therapeutic effect of CBD on knee synovitis. As shown in Figure 8D, TNF-α in model rats was significantly higher than that in naive group, indicating that inflammation was generated in knee synovitis rats. Treatment with CBD-NS DMN could down-regulate serum TNF-α to normal level in knee synovitis rats, while MTX treatment had no observable inhibitory effect on TNF-α. In addition, both CBD-NS DMN and MTX treatments could significantly reduce IL-1β levels. These results indicated that CBD-NS DMN has a good inhibitory effect on TNF-α and IL-1β to reduce inflammation in knee synovitis rats.

Histological Analysis

Pathological changes of knee joints in knee synovitis rats were studied by H&E staining. From Figure 8E, the surface of articular cartilage in normal rats was smooth, chondrocytes were arranged orderly and each layer of synovial membrane structure was clear. In model group, joint tissue structure was moderately abnormal, each layer of synovial tissue structure was unclear and a large number of inflammatory cells infiltrated were observed. Chondrocytes were missing in some areas of the articular cartilage surface in MTX S.C. group and more inflammatory cells infiltrated. After CBD-NS DMN treatment, the cartilage surface was intact and there were fewer inflammatory cells in the synovial membrane and periarticular soft tissues, indicating that CBD-NS DMN had a better therapeutic effect than MTX S.C.

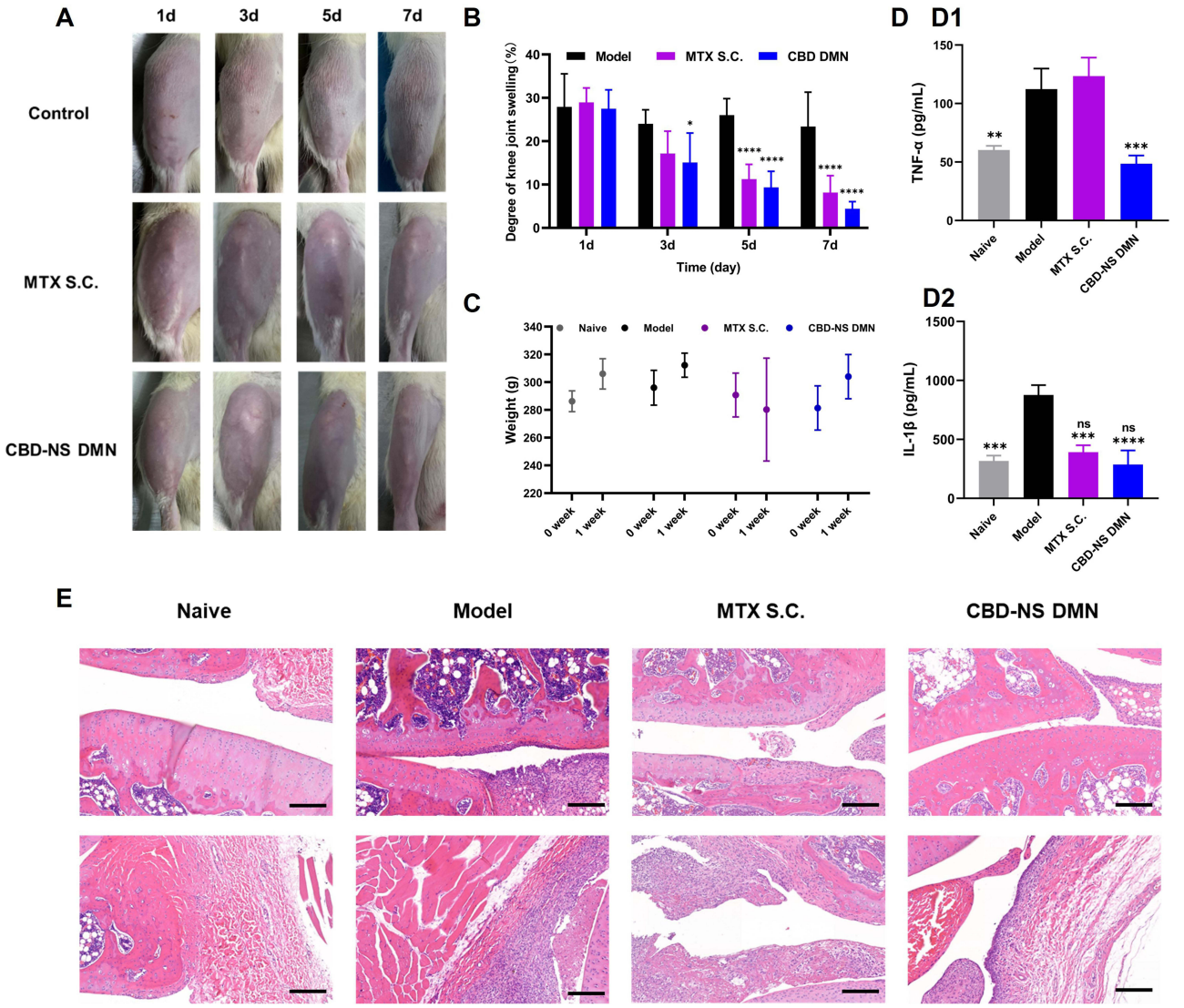

Figure 8 Treatment of rat model of knee synovitis induced by kaolin/λ-carrageenan. (**A**) Images of the knee joints from the Model, MTX S.C. and CBD-NS DMN; (**B**) Statistics of knee swelling degree and (**C**) Changes in body weight of rats after one week of treatment with different groups. (**D**) The serum of rats was used to detect inflammatory factors, including (D1) TNF-α and (D2) IL-1β. (**E**) Histopathological evaluation of knee joint in kaolin/carrageenan-induced knee synovitis model rats. H&E staining images of Naive, Model, MTX S.C. and CBD-NS DMN (Magnification 10×). Scale bar = 200 μm. Data are represented as mean ± S.D., n = 5. The "*" represents the significant difference between each group and the model group, specifically *p < 0.05, **p < 0.01, ***p < 0.001 and ****p < 0.0001. The "ns" represents no significant difference between the groups and the naive group.

Pharmacokinetic Performance of CBD

The pharmacokinetic profiles of CBD in plasma following administration via oral gavage and CBD-NS DMN were elucidated in Figure 9A and B, the pharmacokinetic parameters were shown in Table 3. Distinct trends were observed for the two routes of administration. The oral gavage route exhibited rapid drug absorption, achieving a maximum concentration (C_{max}) of 139.2 ± 42.5 ng/mL at 2 h followed by a swift decline to 40.3 ± 6.2 ng/mL at 4 h, and a gradual decrease to 7.47 ± 1.21 ng/mL by 48 h with no detectable concentration after 60 and 72 h. These outcomes align with previously reported T_{max} and C_{max} values for CBD administered orally.[57] The C_{max} of the CBD-NS DMN group was 144.4 ± 39.4 ng/mL, comparable to the oral gavage group, but notably, the time to reach maximum concentration (T_{max}) was significantly prolonged to 12 h. Additionally, the area under the blood concentration-time curve ($AUC_{0-\infty}$) for the CBD-NS DMN group was 2.47 times greater than that of the oral CBD group. This indicates that CBD-NS DMN administration enhances CBD bioavailability and maintains its plasma concentration for an extended duration.

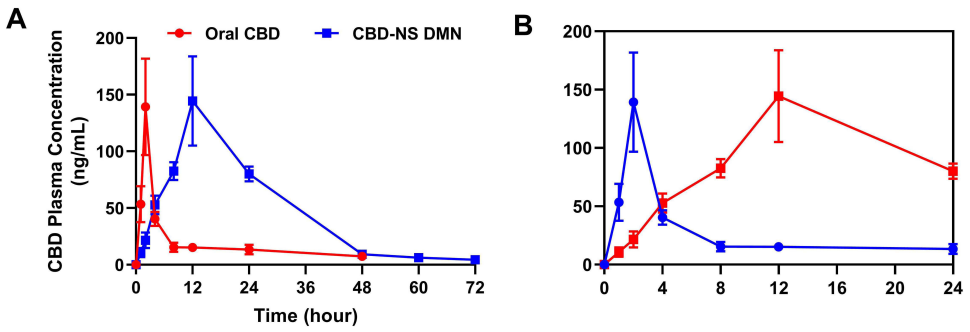

Figure 9 CBD pharmacokinetic curves in the blood of SD rats after oral administration and administration of DMN (**A**) 0–72h; (**B**) 0–24h. Data are represented as mean ± S.D., n = 5.

Discussion

The applicability of TDDS is often constrained by factors such as molecular weight, log P, and the required delivery dose, limiting the spectrum of suitable drug candidates. This limitation is particularly pronounced for highly lipophilic drugs that require high doses, for which traditional TDDS may prove insufficient. NS as a crucial solution for solubilizing these drugs, achieving superior solubility with fewer stabilizing agents. This increased saturation solubility leads to a heightened concentration gradient between the drug and the epidermis, facilitating enhanced passive diffusion.[58] MNs can penetrate the SC barrier and deliver NS to the dermis, this placement allows the NS to act as a reservoir in the dermis, from which the drug can circulate throughout the body.[47] In this study, we integrated NS technology with a DMN delivery system to facilitate the administration of high doses of highly lipophilic drugs, thereby enhancing bioavailability and minimizing the frequency of dosing.

Initially, several stabilizers of CBD-NS were evaluated. Among Tween 80, P127, and HPMC, it was discovered that Tween 80 produced the smallest nanoparticle size, ranging from 100–200 nm. Studies indicate that nanoparticles larger than 100 nm can directly enter host cells through phagocytosis. Furthermore, the smaller the nanocrystal size, the stronger its skin penetration capability.[29] Additionally, the measured zeta potential confirmed that Tween 80 has a stabilizing effect on CBD, preventing nanoparticle aggregation.[59,60]

Numerous studies have explored the incorporation of nanodrugs into DMNs to enhance delivery efficiency.[25,47,56] A one-step manufacturing process was selected for DMN preparation, which enables uniform drug dispersion throughout both the base and the tip, thereby increasing drug loading capacity. This process is straightforward, rapid, and readily scalable for industrial production. Our previous research demonstrated that HA and PVP dissolve more quickly in the skin than PVA and possess favorable mechanical properties, with HA also exhibiting superior biosafety.[61] The addition of trehalose accelerates the dissolution of the tip and contributes to a smoother needle body.[62] HA, PVP, and trehalose were chosen as matrix materials

Table 3 Pharmacokinetic Parameters of CBD in SD Rats After Oral Administration and Administration of DMN (Mean ± S.D., n = 6)

Parameter	Oral	CBD-NS DMN
Dose (mg/kg)	10.0	10.0
C_{max} (ng·mL^{-1})	139.2 ± 42.5	144.4 ± 39.4
T_{max} (h)	2	12
$t_{1/2}$ (h)	0.94	2.3
$AUC_{(0-t)}$ (ng·h·mL^{-1})	899.5	3073.4
$AUC_{(0-\infty)}$ (ng·h·mL^{-1})	1300.0	3215.0

https://doi.org/10.2147/IJN.S452207 DovePress

and combined with CBD-NS to create the DMN. Within just 10 min, the tip of the CBD-NS DMN fully dissolved, indicating successful skin penetration by the CBD-NS alongside the matrix material.

The penetration depth of the MN array into the skin is primarily influenced by the needle height,[63] with taller needles generally achieving deeper penetration. However, this also impacts the mechanical properties, and the delivery efficiency of the MNs.[64] In our study, we opted for MNs with a height of 500 μm. The results of the displacement-force test showed that a single needle could withstand a force exceeding 0.15 N, indicating robust mechanical properties of the CBD-NS DMN.[54] This DMN was capable of penetrating up to 300 μm into the skin, corroborating findings from previous research. Specifically, a DMN fabricated with HA and PVP achieved an insertion depth of 378 μm at a needle height of 500 μm.[21]

CBD-NS is released from the DMN patch following a biphasic release profile, with 80% of the drug being released within 24 h. Consequently, in subsequent experiments, we designated the action time of the DMN patch on the skin as 24 h. Previous studies have shown that CBD typically has limited transdermal permeability. Nonetheless, employing DMN technology substantially improves the delivery efficiency of CBD compared to traditional methods, such as CBD oils and gels.[65–67] In this study, over 1600 μg of CBD-NS was delivered to the rat skin via DMN. Intradermal drug detection indicated that the drug remained at the site of action even after patch removal, with the drug permeating deeper over time and becoming undetectable after 72 h. This suggests that the system is capable of delivering high doses of lipophilic drugs effectively. Furthermore, CBD-NS can act as a reservoir on the skin where it is applied, facilitating deeper drug delivery.

Most pharmacokinetic studies of CBD in animals have been performed through oral or intravenous routes. Lie developed a nano self-emulsifying drug delivery system for oral CBD administration, which achieved a modest increase in bioavailability. However, this method is constrained by its ability to maintain blood levels, typically not exceeding 24 h.[27] Conversely, Paudel introduced a CBD gel incorporating the chemical enhancer Transcutol HP for transdermal application to hairless guinea pigs, successfully maintaining CBD plasma concentrations above 10 ng/mL for up to 100 h.[37] In comparison, the CBD-NS DMN in our study was able to sustain a blood concentration of 10 ng/mL for up to 72 h following patch removal at 24 h, indicating that the drug delivered via DMN remains in the body longer than with oral administration. This suggests a potential reduction in the frequency of dosing. Furthermore, DMN delivery resulted in a shorter duration of action on the skin and higher bioavailability compared to traditional transdermal delivery systems.

In evaluating the anti-inflammatory properties of CBD, this study compared the therapeutic effects of MTX and CBD-NS DMN on knee synovitis. The DMN patch, administered at a dose of 10 mg/kg, led to a significant reduction in swelling after 7 days of treatment. Body weight monitoring revealed a decrease in the body weight of rats in the MTX group, whereas rats treated with CBD-NS DMN displayed a normal weight trend, suggesting good tolerance to CBD-NS DMN. The 10 mg/kg dose provided a useful guideline for the treatment of knee synovitis in subsequent studies. Furthermore, CBD's potent anti-inflammatory action effectively suppressed inflammatory markers such as TNF-α and IL-1β in knee synovitis rats, bringing them back to normal levels, aligning with findings from prior research.[35]

Utilizing CBD as a model drug, we have successfully developed the drug-NS DMN platform. The combined properties of HA, PVP, and trehalose resulted in a DMN with optimal dissolution, mechanical strength, and skin permeation characteristics. Future research will explore the application of this platform to other lipophilic drugs, further demonstrating its broad applicability.

Conclusion

The traditional TDDS often faces limitations related to factors such as molecular weight, log P, and dosage requirements. MNs present a significant advancement in overcoming these challenges. In our study, we developed a DMN patch specifically tailored for the delivery of highly lipophilic drugs, facilitating high-dose administration. CBD was selected as the model drug for this endeavor. Initially, a NS with a high concentration of CBD was prepared using bottom-up technology, which was then integrated with the matrix material to create the DMN. The inclusion of HA, PVP, and trehalose significantly improved the DMN's intradermal dissolution capabilities and mechanical strength. Impressively, the CBD-NS DMN exhibited superior drug release and intradermal delivery, administering 80% of the drug within 24 h. Pharmacodynamic outcomes demonstrated that CBD-NS DMN surpassed MTX in terms of efficacy and safety for knee synovitis treatment, also showing an inhibitory effect on TNF-α and IL-1β in knee synovitis rats. Compared to conventional oral administration, CBD-NS DMN enhanced CBD permeation through the skin, prolonged action time,

and increased bioavailability. This novel delivery system emerges as an effective strategy for administering highly lipophilic drugs like CBD, enabling high-dose delivery.

Abbreviations

TDDS, transdermal drug delivery system; DMN, dissolving microneedle; NS, nanosuspensions; PDI, polydispersity index; SD, Sprague-Dawley; SC, stratum corneum; MNs, microneedles; NCs, nanocrystals; CBD, cannabidiol; Tween 80, polysorbate 80; P127, Pluronic® F-127; HPMC, hydroxypropyl methylcellulose; PVP, polyvinylpyrrolidone; HA, hyaluronic acid; ACN, acetonitrile; DI, deionized; SEM, scanning electron microscopy; TEM, transmission electron microscopy; DSC, differential scanning calorimetry; XRD, powder x-ray diffraction; C6, coumarin 6; CLSM, confocal laser scanning microscope; EP, Eppendorf; S.D., standard deviation; 3D, three-dimensional.

Acknowledgments

We gratefully acknowledge the financial support of the Science and Technology Service Network Initiative of the Chinese Academy of Sciences, China (KFJ-STS-QYZD-182).

Disclosure

The authors report no conflicts of interest in this work.

References

1. Paredes AJ, McKenna PE, Ramöller IK, et al. Microarray patches: poking a hole in the challenges faced when delivering poorly soluble drugs. *Adv Funct Mater*. 2020;31(1). doi:10.1002/adfm.202005792
2. Sengupta P, Chatterjee B. Potential and future scope of nanoemulgel formulation for topical delivery of lipophilic drugs. *Int J Pharm*. 2017;526(1–2):353–365. doi:10.1016/j.ijpharm.2017.04.068
3. Zhang LH, Zhu WF, Lin QS, Han J, Jiang LQ, Zhang YZ. Hydroxypropyl-β-cyclodextrin functionalized calcium carbonate microparticles as a potential carrier for enhancing oral delivery of water-insoluble drugs. *Int J Nanomed*. 2015;10:3291–3302. doi:10.2147/Ijn.S78814
4. Mbah CC, Builders PF, Attama AA. Nanovesicular carriers as alternative drug delivery systems: ethosomes in focus. *Expert Opin Drug Deliv*. 2014;11(1):45–59. doi:10.1517/17425247.2013.860130
5. Chen H, Khemtong C, Yang X, Chang X, Gao J. Nanonization strategies for poorly water-soluble drugs. *Drug Discovery Today*. 2011;16(7–8):354–360. doi:10.1016/j.drudis.2010.02.009
6. Pandey RP, Vidic J, Mukherjee R, Chang CM. Experimental methods for the biological evaluation of nanoparticle-based drug delivery risks. *Pharmaceutics*. 2023;15(2). doi:10.3390/pharmaceutics15020612
7. Kalepu S, Nekkanti V. Insoluble drug delivery strategies: review of recent advances and business prospects. *Acta Pharmaceutica Sinica B*. 2015;5(5):442–453. doi:10.1016/j.apsb.2015.07.003
8. Bird D, Ravindra NM. Transdermal drug delivery and patches—An overview. *Med Dev Sensors*. 2020;3(6). doi:10.1002/mds3.10069
9. Siavashy S, Soltani M, Ahmadi M, Landi B, Mehmanparast H, Ghorbani-Bidkorbeh F. A comprehensive review of one decade of microfluidic platforms applications in synthesis of enhanced carriers utilized in controlled drug delivery. *Adv Mater Technol*. 2022;7(10). doi:10.1002/admt.202101615
10. Tijani AO, Thakur D, Mishra D, Frempong D, Chukwunyere UI, Puri A. Delivering therapeutic cannabinoids via skin: current state and future perspectives. *J Control Release*. 2021;334:427–451. doi:10.1016/j.jconrel.2021.05.005
11. Fu XL, Shi YB, Wang H, et al. Ethosomal gel for improving transdermal delivery of thymosin β-4. *Int j Nanomed*. 2019;14:9275–9284. doi:10.2147/Ijn.S228863
12. Li B, Lu G, Liu W, Liao L, Ban J, Lu Z. Formulation and evaluation of PLGA nanoparticulate-based microneedle system for potential treatment of neurological diseases. *Int j Nanomed*. 2023;18:3745–3760. doi:10.2147/ijn.S415728
13. Swain S, Beg S, Singh A, Patro CN, Rao MEB. Advanced techniques for penetration enhancement in transdermal drug delivery system. *Curr Drug Deliv*. 2011;8(4):456–473. doi:10.2174/156720111795767979
14. Prausnitz MR, Langer R. Transdermal drug delivery. *Nature Biotechnol*. 2008;26(11):1261–1268. doi:10.1038/nbt.1504
15. Xu Y, Zhao M, Cao J, et al. Applications and recent advances in transdermal drug delivery systems for the treatment of rheumatoid arthritis. *Acta Pharmaceutica Sinica B*. 2023. doi:10.1016/j.apsb.2023.05.025
16. Funke AP, Günther C, Müller RH, Lipp R. Development of matrix patches for transdermal delivery of a highly lipophilic antiestrogen. *Drug Dev Ind Pharm*. 2003;29(7):785–793. doi:10.1081/ddc-120021778
17. Lee KJ, Jeong SS, Roh DH, Kim DY, Choi HK, Lee EH. A practical guide to the development of microneedle systems - In clinical trials or on the market. *Int J Pharm*. 2020;573:118778. doi:10.1016/j.ijpharm.2019.118778
18. Salwa, Chevala NT, Jitta SR, Marques SM, Vaz VM, Kumar L. Polymeric microneedles for transdermal delivery of nanoparticles: frontiers of formulation, sterility and stability aspects. *J Drug Delivery Sci Technol*. 2021;65. doi:10.1016/j.jddst.2021.102711
19. Karim Z, Karwa P, Hiremath SRR. Polymeric microneedles for transdermal drug delivery- A review of recent studies. *J Drug Delivery Sci Technol*. 2022;77. doi:10.1016/j.jddst.2022.103760
20. Bauleth-Ramos T, El-Sayed N, Fontana F, Lobita M, Shahbazi M-A, Santos HA. Recent approaches for enhancing the performance of dissolving microneedles in drug delivery applications. *Mater Today*. 2023;63:239–287. doi:10.1016/j.mattod.2022.12.007

21. González-Vázquez P, Larrañeta E, McCrudden MTC, et al. Transdermal delivery of gentamicin using dissolving microneedle arrays for potential treatment of neonatal sepsis. *J Control Release*. 2017;265:30–40. doi:10.1016/j.jconrel.2017.07.032
22. Wu Y, Vora LK, Mishra D, et al. Nanosuspension-loaded dissolving bilayer microneedles for hydrophobic drug delivery to the posterior segment of the eye. *Biomater Adv*. 2022:137. doi:10.1016/j.bioadv.2022.212767
23. Dangol M, Yang H, Li CG, et al. Innovative polymeric system (IPS) for solvent-free lipophilic drug transdermal delivery via dissolving microneedles. *J Control Release*. 2016;223:118–125. doi:10.1016/j.jconrel.2015.12.038
24. Al-Kassas R, Bansal M, Shaw J. Nanosizing techniques for improving bioavailability of drugs. *J Control Release*. 2017;260:202–212. doi:10.1016/j.jconrel.2017.06.003
25. Wei F, Wang Q, Liu H, et al. High efficacy combined microneedles array with methotrexate nanocrystals for effective anti-rheumatoid arthritis. *Int j Nanomed*. 2022;17:2397–2412. doi:10.2147/ijn.S365523
26. Aparicio-Blanco J, Sebastián V, Benoit JP, Torres-Suárez AI. Lipid nanocapsules decorated and loaded with cannabidiol as targeted prolonged release carriers for glioma therapy: in vitro screening of critical parameters. *Eur J Pharm Biopharm*. 2019;134:126–137. doi:10.1016/j.ejpb.2018.11.020
27. Kok LY, Bannigan P, Sanaee F, et al. Development and pharmacokinetic evaluation of a self-nanoemulsifying drug delivery system for the oral delivery of cannabidiol. *Eur J Pharm Sci*. 2022:168. doi:10.1016/j.ejps.2021.106058
28. Rao Y, Li R, Liu S, et al. Enhanced bioavailability and biosafety of cannabidiol nanomicelles for effective anti-inflammatory therapy. *Particuology*. 2022;69:1–9. doi:10.1016/j.partic.2021.11.010
29. Parmar PK, Wadhawan J, Bansal AK. Pharmaceutical nanocrystals: a promising approach for improved topical drug delivery. *Drug Discovery Today*. 2021;26(10):2329–2349. doi:10.1016/j.drudis.2021.07.010
30. Pisanti S, Malfitano AM, Ciaglia E, et al. Cannabidiol: state of the art and new challenges for therapeutic applications. *Pharmacol Ther*. 2017;175:133–150. doi:10.1016/j.pharmthera.2017.02.041
31. Li H, Liu Y, Tian D, et al. Overview of cannabidiol (CBD) and its analogues: structures, biological activities, and neuroprotective mechanisms in epilepsy and Alzheimer's disease. *Eur J Med Chem*. 2020:192. doi:10.1016/j.ejmech.2020.112163
32. Bruni N, Della Pepa C, Oliaro-Bosso S, Pessione E, Gastaldi D, Dosio F. Cannabinoid delivery systems for pain and inflammation treatment. *Molecules*. 2018;23(10). doi:10.3390/molecules23102478
33. Hao F, Feng Y. Cannabidiol (CBD) enhanced the hippocampal immune response and autophagy of APP/PS1 Alzheimer's mice uncovered by RNA-seq. *Life Sci*. 2021;264. doi:10.1016/j.lfs.2020.118624
34. Nichols JM, Kaplan BLF. Immune responses regulated by cannabidiol. *Cannabis Cannabinoid Res*. 2020;5(1):12–31. doi:10.1089/can.2018.0073
35. Malfait AM, Gallily R, Sumariwalla PF, et al. The nonpsychoactive cannabis constituent cannabidiol is an oral anti-arthritic therapeutic in murine collagen-induced arthritis. *Proc Natl Acad Sci*. 2000;97(17):9561–9566. doi:10.1073/pnas.160105897
36. Philpott HT, O'Brien M, McDougall JJ. Attenuation of early phase inflammation by cannabidiol prevents pain and nerve damage in rat osteoarthritis. *Pain*. 2017;158(12):2442–2451. doi:10.1097/j.pain.0000000000001052
37. Hammell DC, Zhang LP, Ma F, et al. Transdermal cannabidiol reduces inflammation and pain-related behaviours in a rat model of arthritis. *Eur J Pain*. 2016;20(6):936–948. doi:10.1002/ejp.818
38. Lodzki M, Godin B, Rakou L, Mechoulam R, Gallily R, Touitou E. Cannabidiol—transdermal delivery and anti-inflammatory effect in a murine model. *J Control Release*. 2003;93(3):377–387. doi:10.1016/j.jconrel.2003.09.001
39. Pirrung MC. Synthetic access to cannabidiol and analogs as active pharmaceutical ingredients. *J Med Chem*. 2020;63(21):12131–12136. doi:10.1021/acs.jmedchem.0c00095
40. Pang L, Zhu S, Ma J, et al. Intranasal temperature-sensitive hydrogels of cannabidiol inclusion complex for the treatment of post-traumatic stress disorder. *Acta Pharmaceutica Sinica B*. 2021;11(7):2031–2047. doi:10.1016/j.apsb.2021.01.014
41. Izgelov D, Davidson E, Barasch D, Regev A, Domb AJ, Hoffman A. Pharmacokinetic investigation of synthetic cannabidiol oral formulations in healthy volunteers. *Eur J Pharm Biopharm*. 2020;154:108–115. doi:10.1016/j.ejpb.2020.06.021
42. Volpe-Zanutto F, Ferreira LT, Permana AD, et al. Artemether and lumefantrine dissolving microneedle patches with improved pharmacokinetic performance and antimalarial efficacy in mice infected with Plasmodium yoelii. *J Control Release*. 2021;333:298–315. doi:10.1016/j.jconrel.2021.03.036
43. Möschwitzer JP. Drug nanocrystals in the commercial pharmaceutical development process. *Int J Pharm*. 2013;453(1):142–156. doi:10.1016/j.ijpharm.2012.09.034
44. Wang Q, Yang X, Gu X, et al. Celecoxib nanocrystal-loaded dissolving microneedles with highly efficient for osteoarthritis treatment. *Int J Pharm*. 2022:625. doi:10.1016/j.ijpharm.2022.122108
45. Abdelghany S, Tekko IA, Vora L, Larrañeta E, Permana AD, Donnelly RF. Nanosuspension-based dissolving microneedle arrays for intradermal delivery of curcumin. *Pharmaceutics*. 2019;11(7). doi:10.3390/pharmaceutics11070308
46. He M, Yang G, Zhang S, Zhao X, Gao Y. Dissolving microneedles loaded with etonogestrel microcrystal particles for intradermal sustained delivery. *J Pharmaceut Sci*. 2018;107(4):1037–1045. doi:10.1016/j.xphs.2017.11.013
47. Vora LK, Vavia PR, Larrañeta E, Bell SEJ, Donnelly RF. Novel nanosuspension-based dissolving microneedle arrays for transdermal delivery of a hydrophobic drug. *J Interdiscip Nanomed*. 2018;3(2):89–101. doi:10.1002/jin2.41
48. Yu K, Yu X, Cao S, et al. Layered dissolving microneedles as a need-based delivery system to simultaneously alleviate skin and joint lesions in psoriatic arthritis. *Acta Pharmaceutica Sinica B*. 2021;11(2):505–519. doi:10.1016/j.apsb.2020.08.008
49. Wang B, Zhang S, Yang G, et al. Dissolvable polymeric microneedles loaded with aspirin for antiplatelet aggregation. *Asian J Pharm Sci*. 2023;18(1). doi:10.1016/j.ajps.2023.100776
50. Vargas-Ruiz R, Montiel-Ruiz RM, Herrera-Ruiz M, et al. Effect of phenolic compounds from Oenothera rosea on the kaolin-carrageenan induced arthritis model in mice. *J Ethnopharmacol*. 2020:253. doi:10.1016/j.jep.2020.112711
51. Tuomela A, Hirvonen J, Peltonen L. Stabilizing agents for drug nanocrystals: effect on bioavailability. *Pharmaceutics*. 2016;8(2). doi:10.3390/pharmaceutics8020016
52. Chogale M, Ghodake V, Patravale V. Performance parameters and characterizations of nanocrystals: a brief review. *Pharmaceutics*. 2016;8(3). doi:10.3390/pharmaceutics8030026

53. Bansal V, Demir YK, Akan Z, Kerimoglu O. Characterization of polymeric microneedle arrays for transdermal drug delivery. *PLoS One*. 2013;8 (10). doi:10.1371/journal.pone.0077289
54. Li W, Terry RN, Tang J, Feng MR, Schwendeman SP, Prausnitz MR. Rapidly separable microneedle patch for the sustained release of a contraceptive. *Nat Biomed Eng*. 2019;3(3):220–229. doi:10.1038/s41551-018-0337-4
55. Matarazzo AP, Elisei LMS, Carvalho FC, et al. Mucoadhesive nanostructured lipid carriers as a cannabidiol nasal delivery system for the treatment of neuropathic pain. *Eur J Pharm Sci*. 2021:159. doi:10.1016/j.ejps.2020.105698
56. Tekko IA, Permana AD, Vora L, Hatahet T, McCarthy HO, Donnelly RF. Localised and sustained intradermal delivery of methotrexate using nanocrystal-loaded microneedle arrays: potential for enhanced treatment of psoriasis. *Eur J Pharm Sci*. 2020;152. doi:10.1016/j.ejps.2020.105469
57. Xu C, Chang T, Du Y, Yu C, Tan X, Li X. Pharmacokinetics of oral and intravenous cannabidiol and its antidepressant-like effects in chronic mild stress mouse model. *Environ Toxicol Pharmacol*. 2019;70. doi:10.1016/j.etap.2019.103202
58. Parveen N, Abourehab MAS, Thanikachalam PV, Khar RK, Kesharwani P. Nanocrystals as an emerging nanocarrier for the management of dermatological diseases. *Colloids Surf B*. 2023;225. doi:10.1016/j.colsurfb.2023.113231
59. Verma S, Huey BD, Burgess DJ. Scanning probe microscopy method for nanosuspension stabilizer selection. *Langmuir*. 2009;25(21):12481–12487. doi:10.1021/la9016432
60. Dolenc A, Kristl J, Baumgartner S, Planinsek O. Advantages of celecoxib nanosuspension formulation and transformation into tablets. *Int J Pharm*. 2009;376(1–2):204–212. doi:10.1016/j.ijpharm.2009.04.038
61. Cheng AG, Sun WT, Xing MZ, Zhang SH, Gao YH. The hygroscopicity of polymer microneedles on the performance of dissolving behavior for transdermal delivery. *Int J Polym Mater Po*. 2022;71(1):72–78. doi:10.1080/00914037.2020.1798442
62. Zhao X, Zhang S, Yang G, Zhou Z, Gao Y. Exploring trehalose on the release of levonorgestrel from implantable PLGA microneedles. *Polymers*. 2020;12(1). doi:10.3390/polym12010059
63. Zhou Y, Yang L, Lyu Y, et al. Topical delivery of ROS-responsive methotrexate prodrug nanoassemblies by a dissolvable microneedle patch for psoriasis therapy. *Int J Nanomed*. 2023;18:899–915. doi:10.2147/ijn.S394957
64. Li W, Li S, Fan X, Prausnitz MR. Microneedle patch designs to increase dose administered to human subjects. *J Control Release*. 2021;339:350–360. doi:10.1016/j.jconrel.2021.09.036
65. Paudel KS, Hammell DC, Agu RU, Valiveti S, Stinchcomb AL. Cannabidiol bioavailability after nasal and transdermal application: effect of permeation enhancers. *Drug Dev Ind Pharm*. 2010;36(9):1088–1097. doi:10.3109/03639041003657295
66. Stinchcomb AL, Valiveti S, Hammell DC, Ramsey DR. Human skin permeation of Δ8-tetrahydrocannabinol, cannabidiol and cannabinol. *J Pharm Pharmacol*. 2004;56(3):291–297. doi:10.1211/0022357022791
67. Junaid MSA, Tijani AO, Puri A, Banga AK. In vitro percutaneous absorption studies of cannabidiol using human skin: exploring the effect of drug concentration, chemical enhancers, and essential oils. *Int J Pharm*. 2022;616. doi:10.1016/j.ijpharm.2022.121540